

Chapter 3

Collapsing condensates and atomic bursts

3.1 Outlook

Having thoroughly discussed the two-body physics underlying Feshbach resonant interactions, we are now in a position to apply these ideas to a many-body system. We begin, in this chapter, by discussing the formalism for Bosons and apply it to a particularly novel experiment. In the next chapter we will expand upon this formalism to account for Fermions.

3.2 The “Bosenova” problem in collapsing condensates

The ability to dynamically modify the nature of the microscopic interactions in a Bose-Einstein condensate—an ability virtually unique to the field of dilute gases—opens the way to the exploration of a range of fundamental phenomena. A striking example of this is the “Bosenova” experiment carried out in the Wieman group at JILA [39] which explored the mechanical collapse instability arising from an attractive interaction. This collapse resulted in an unanticipated burst of atoms, the nature of which is a subject of current debate.

The Bosenova experiment, conducted by the JILA group, consisted of the following elements. A conventional, stable Bose-Einstein condensate was created in equilibrium. The group then used a Feshbach resonance to abruptly switch the interactions to be attractive inducing an implosion. One might have predicted that the rapid in-

crease in density would simply lead to a rapid loss of atoms, primarily through inelastic three-body collisions. In contrast, what was observed was the formation of an energetic burst of atoms emerging from the center of the implosion. Although the energy of these atoms was much larger than that of the condensate, the energy was insignificant when compared to the molecular binding energy which characterizes the energy released in a three-body collision. In the end, what remained was a remnant condensate which appeared distorted and was believed to be in a highly excited collective state.

One theoretical method which has been extensively explored to explain this behavior has been the inclusion of a decay term into the Gross-Pitaevskii equation as a way to account for the atom loss [40, 41, 42, 43]. Aside from its physical application to the Bose-nova problem, the inclusion of three-body loss as a phenomenological mechanism represents an important mathematical problem, since the nonlinear Gross-Pitaevskii equation allows for a class of self-similar solutions in the unstable regime. The local collapses predicted in this framework can generate an outflow even within this zero temperature theory. However, there are a number of aspects which one should consider when applying the extended Gross-Pitaevskii equation to account for the observations made in the JILA experiment.

The first problematic issue is the potential breakdown of the principle of attenuation of correlations. This concept is essential in any quantum or classical kinetic theory as it allows multi-particle correlations to be factorized. The assumption of attenuation of correlations is especially evident in the derivation of the Gross-Pitaevskii equation where all explicit multi-particle correlations are dropped. Furthermore, there is considerable evidence for this instability toward pair formation in the mechanically unstable quantum theory [44].

A second difficulty with motivating the Gross-Pitaevskii approach is that, by this method, one describes the energy-dependent interactions through a single parameter, the scattering length, which is determined from the s -wave scattering phase shift at

zero scattering energy. Near a Feshbach resonance, as we have seen in Chapter 1, the proximity of a bound state in a closed potential to the zero of the scattering continuum can lead to a strong energy dependence of the scattering. Exactly on resonance, the s -wave scattering length passes through infinity and, in this situation, the Gross-Pitaevskii equation is undefined.

These two fundamental difficulties with the Gross-Pitaevskii approach led us to reconsider the Bosenova problem [45]. We were motivated by the fact that the same experimental group at JILA recently performed a complementary experiment [19]—the, so called, molecular Ramsey fringe experiment. Their results provided significant insight into this problem. What was remarkable in these new experiments was that, even with a large positive scattering length, in which the interactions were repulsive, a burst of atoms and a remnant condensate were observed. Furthermore, in the large positive scattering length case, simple effective field theories, which included an explicit description of the Feshbach resonance physics, were able to provide an accurate quantitative comparison with the data [46, 47, 48]. The theory showed the burst to arise from the complex dynamics of the atom condensate which was coupled to a coherent field of exotic molecular dimers of a remarkable physical size and near the threshold binding energy.

In this Chapter, based on the work of [45], we draw connections between the two JILA experiments. We pose and resolve the question as to whether the burst of atoms in the Bosenova collapse could arise in a similar way as in the Ramsey fringe experiment—from the formation of a coherent molecular superfluid. This hypothesis is tested by applying an effective field theory for resonance superfluidity to the collapse. For fermions, the case of resonance superfluidity in an inhomogeneous system has been treated in the local density approximation using, essentially, the uniform solution at each point in space [49]. For the collapse of a Bose-Einstein condensate, as we wish to treat here, the local density approximation is not valid and the calculation must be

performed on a truly inhomogeneous system.

3.3 Development of an effective field theory for bosons

In the Feshbach resonance illustrated in Figure 1.1, the properties of the collision of two ground state atoms is controlled through their resonant coupling to a bound state in a closed channel Born-Oppenheimer potential. By adjusting an external magnetic field, the scattering length can be tuned to have any value. This field dependence of the scattering length is characterized by the detuning $\bar{\nu}$ and obeys a dispersive profile given by $a(\bar{\nu}) = a_{\text{bg}}(1 - \kappa/(2\bar{\nu}))$, with κ the resonance width and a_{bg} the background scattering length. In fact, as described in Chapter 2.1, all the scattering properties of a Feshbach resonance system are completely characterized by just three parameters $\bar{U} = 4\pi\hbar^2 a_{\text{bg}}/m$, $\bar{g} = \sqrt{\kappa\bar{U}}$, and $\bar{\nu}$. Physically, \bar{U} represents the energy shift per unit density on the single particle eigenvalues due to the background scattering processes, while \bar{g} , which has dimensions of energy per square-root density, represents the coupling of the Feshbach resonance between the open and closed channel potentials.

We now proceed to construct a low order many-body theory which includes this resonance physics. The Hamiltonian for a dilute gas of scalar bosons with binary interactions is given in complete generality by

$$H = \int d^3x \psi_a^\dagger(\mathbf{x}) H_a(\mathbf{x}) \psi_a(\mathbf{x}) + \frac{1}{2} \int d^3x d^3x' \psi_a^\dagger(\mathbf{x}) \psi_a^\dagger(\mathbf{x}') U(\mathbf{x}, \mathbf{x}') \psi_a(\mathbf{x}') \psi_a(\mathbf{x}), \quad (3.1)$$

where $H_a(\mathbf{x})$ is the single particle Hamiltonian, $U(\mathbf{x}, \mathbf{x}')$ is the binary interaction potential, and $\psi_a(\mathbf{x})$ is a bosonic scalar field operator. In cold quantum gases, where the atoms collide at very low energy, we are only interested in the behavior of the scattering about a small energy range above zero. There exist many potentials which replicate the low energy scattering behavior of the true potential; therefore, it is convenient to carry out the calculation with the simplest one, the most convenient choice being to take the interaction potential as a delta-function pseudo-potential when possible.

For a Feshbach resonance, this choice of pseudo-potential is generally not available since the energy dependence of the scattering implies that a minimal treatment must at least contain a spread of wave-numbers which is equivalent to the requirement of a non-local potential. Since the solution of a nonlocal field theory is inconvenient, we take an alternative, but equivalent, approach. We include into the theory an auxiliary molecular field operator $\psi_m(\mathbf{x})$ which obeys Bose statistics and describes the collision between atoms in terms of two elementary components: i.) the background collisions between atoms in the absence of the resonance interactions and ii.) the conversion of atom pairs into tightly bound, molecular states. This allows us to construct a local field theory with the property that when this auxiliary field is integrated out, an effective Hamiltonian of the form given in Eq. (3.1) is recovered with a potential $V(\mathbf{x}, \mathbf{x}') = V(|\mathbf{x} - \mathbf{x}'|)$ which generates the form of the two-body T -matrix predicted by Feshbach resonance theory (Eq. (2.20) with (2.25)). The local Hamiltonian which generates this scattering behavior is:

$$\begin{aligned}
H &= \int d^3x \psi_a^\dagger(\mathbf{x}) H_a(x) \psi_a(\mathbf{x}) + \int d^3x \psi_m^\dagger(\mathbf{x}) H_m(x) \psi_m(\mathbf{x}) \\
&+ \frac{1}{2} \int d^3x d^3x' \psi_a^\dagger(\mathbf{x}) \psi_a^\dagger(\mathbf{x}') U(\mathbf{x} - \mathbf{x}') \psi_a(\mathbf{x}) \psi_a(\mathbf{x}') \\
&+ \frac{1}{2} \int d^3x d^3x' \left(\psi_m^\dagger\left(\frac{\mathbf{x} + \mathbf{x}'}{2}\right) g(\mathbf{x} - \mathbf{x}') \psi_a(\mathbf{x}) \psi_a(\mathbf{x}') + \text{h.c.} \right). \quad (3.2)
\end{aligned}$$

Equation (3.2) has the intuitive structure of resonant atom-molecule coupling [50, 51] and was motivated by bosonic models of superfluidity [52, 53]. Here we have defined the free atomic dispersion $H_a(x) = -\frac{\hbar^2}{2m} \nabla_x^2 + V_a(\mathbf{x}) - \mu_a$ and the free molecular dispersion $H_m(x) = -\frac{\hbar^2}{4m} \nabla_x^2 + V_m(\mathbf{x}) - \mu_m$. $V_{a,m}$ are the external potentials and $\mu_{a,m}$ are the chemical potentials (the subscripts a, m represent the atomic and molecular contributions, respectively). The Feshbach resonance is controlled by the magnetic field which is incorporated into the theory by the detuning $\nu = \mu_m - 2\mu_a$ between the atomic and molecular fields.

The field operators which we have introduced $\psi_a^\dagger(\mathbf{x}), \psi_a(\mathbf{x})$ create and destroy

atoms at point \mathbf{x} and $\psi_m^\dagger(\mathbf{x}), \psi_m(\mathbf{x})$ create and destroy molecules at point \mathbf{x} . For the bosonic gas, both sets of these operators obey Bose commutation relations:

$$\begin{aligned} [\psi_a(\mathbf{x}), \psi_a^\dagger(\mathbf{x}')] &= \delta^3(\mathbf{x} - \mathbf{x}') \\ [\psi_m(\mathbf{x}), \psi_m^\dagger(\mathbf{x}')] &= \delta^3(\mathbf{x} - \mathbf{x}'), \end{aligned} \quad (3.3)$$

and we assume that the fields ψ_a and ψ_m commute. It is important to keep in mind that the parameters introduced in the field theory are distinct from the physical parameters \bar{U} , \bar{g} , and $\bar{\nu}$ behind the resonance. In order for the local Hamiltonian given in Eq. (3.2) to be applicable, one must introduce into the field theory a renormalized set of parameters. Since we will be working with contact potentials, each will contain a momentum cutoff associated with a maximum wavenumber K_c . This need not be physical in origin but should exceed the momentum range of occupied quantum states. The relationships between the renormalized and physical parameters for the contact potentials are given in Appendix A.1. Of course, all of our final results must be independent of this artificial cutoff; a condition which has been checked for all the results we will present.

To begin our development of a resonant field theory, we define the atomic and molecular condensates in terms of the mean-fields of their respective operators

$$\phi_a(\mathbf{x}) = \langle \psi_a(\mathbf{x}) \rangle \quad \text{and} \quad \phi_m(\mathbf{x}) = \langle \psi_m(\mathbf{x}) \rangle. \quad (3.4)$$

The remainder is associated with the fluctuations about these mean-fields and can likewise be defined:

$$\chi_a(\mathbf{x}) = \psi_a(\mathbf{x}) - \phi_a(\mathbf{x}) \quad \text{and} \quad \chi_m(\mathbf{x}) = \psi_m(\mathbf{x}) - \phi_m(\mathbf{x}). \quad (3.5)$$

Assuming the occupation of $\phi_m(\mathbf{x})$ to be small (less than 2% in the simulations we present), we drop higher-order terms arising from fluctuations about this mean-field which do not give a significant correction to our results.

Starting from Heisenberg's equation of motion

$$i \frac{\partial}{\partial t} A(\mathbf{x}, t) = [A(\mathbf{x}, t), H(\mathbf{x}', t')], \quad (3.6)$$

we may derive a hierarchy of time dependent equations for the various fields involved within our problem, each coupling to higher-order correlations. To truncate this hierarchy, we work within Hartree-Fock-Bogoliubov (HFB) theory. The simplification which this introduces into the problem is that it allows us to factorize terms to quadratic order in the field operators. Another way to say this is that we only account for correlations between pairs of fields, but neglect all higher-order correlations. For example, we use Wick's theorem to factorize a four-point interaction as:

$$\begin{aligned} \langle A(\mathbf{x}_1)A(\mathbf{x}_2)A(\mathbf{x}_3)A(\mathbf{x}_4) \rangle &= \langle A(\mathbf{x}_1)A(\mathbf{x}_2) \rangle \langle A(\mathbf{x}_3)A(\mathbf{x}_4) \rangle \\ &+ \langle A(\mathbf{x}_1)A(\mathbf{x}_3) \rangle \langle A(\mathbf{x}_2)A(\mathbf{x}_4) \rangle + \langle A(\mathbf{x}_1)A(\mathbf{x}_4) \rangle \langle A(\mathbf{x}_2)A(\mathbf{x}_3) \rangle. \end{aligned} \quad (3.7)$$

Under this set of approximations we derive four equations: two corresponding to a Schrödinger evolution of the mean fields

$$\begin{aligned} i\hbar \frac{d\phi_a(\mathbf{x})}{dt} &= \left(-\frac{\hbar^2}{2m} \nabla_{\mathbf{x}}^2 + V_a(\mathbf{x}) - \mu_a + U[|\phi_a(\mathbf{x})|^2 + 2G_N(\mathbf{x}, \mathbf{x})] \right) \phi_a(\mathbf{x}) \\ &+ [UG_A(\mathbf{x}, \mathbf{x}) + g\phi_m(\mathbf{x})] \phi_a^*(\mathbf{x}), \end{aligned} \quad (3.8)$$

$$i\hbar \frac{d\phi_m(\mathbf{x})}{dt} = \left(-\frac{\hbar^2}{4m} \nabla_{\mathbf{x}}^2 + V_m(\mathbf{x}) - \mu_m \right) \phi_m(\mathbf{x}) + \frac{g}{2} [\phi_a^2(\mathbf{x}) + G_A(\mathbf{x}, \mathbf{x})], \quad (3.9)$$

and two corresponding to the Liouville space evolution of the normal density $G_N(\mathbf{x}, \mathbf{x}') = \langle \chi_a^\dagger(\mathbf{x}') \chi_a(\mathbf{x}) \rangle$ and of the anomalous density $G_A(\mathbf{x}, \mathbf{x}') = \langle \chi_a(\mathbf{x}') \chi_a^\dagger(\mathbf{x}) \rangle$. The time evolution of the densities may be expressed in the compact form [54]

$$i\hbar \frac{\partial \mathcal{G}}{\partial t} = \Sigma \mathcal{G} - \mathcal{G} \Sigma^\dagger, \quad (3.10)$$

where the density matrix and self-energy matrix are defined respectively as

$$\mathcal{G}(\mathbf{x}, \mathbf{x}') = \begin{pmatrix} \langle \chi_a^\dagger(\mathbf{x}') \chi_a(\mathbf{x}) \rangle & \langle \chi_a(\mathbf{x}') \chi_a(\mathbf{x}) \rangle \\ \langle \chi_a^\dagger(\mathbf{x}') \chi_a^\dagger(\mathbf{x}) \rangle & \langle \chi_a(\mathbf{x}') \chi_a^\dagger(\mathbf{x}) \rangle \end{pmatrix}, \quad (3.11)$$

and

$$\Sigma(\mathbf{x}, \mathbf{x}') = \begin{pmatrix} H(\mathbf{x}, \mathbf{x}') & \Delta(\mathbf{x}, \mathbf{x}') \\ -\Delta^*(\mathbf{x}, \mathbf{x}') & -H^*(\mathbf{x}, \mathbf{x}') \end{pmatrix}. \quad (3.12)$$

The convenience of choosing a microscopic model in which the potential couplings are of contact form is now evident since the elements of the self-energy matrix Σ are diagonal in \mathbf{x} and \mathbf{x}' with non-zero elements

$$\begin{aligned} H(\mathbf{x}, \mathbf{x}) &= -\frac{\hbar^2}{2m}\nabla_x^2 + V_a(\mathbf{x}) - \mu_a + 2U[|\phi_a(\mathbf{x})|^2 + G_N(\mathbf{x}, \mathbf{x})], \\ \Delta(\mathbf{x}, \mathbf{x}) &= U[\phi_a^2(\mathbf{x}) + G_A(\mathbf{x}, \mathbf{x})] + g\phi_m(\mathbf{x}). \end{aligned} \quad (3.13)$$

3.4 Application to a spherical trap geometry

Equations (3.8), (3.9), and (3.10) form a closed set of equations for the inhomogeneous system. However, since the normal density and anomalous pairing field are both six-dimensional objects, it is very difficult to solve these equations in an arbitrary geometry. For this reason, we consider the case of greatest symmetry consisting of a spherical trap. Here we can reduce the problem to one of only three dimensions according to the following procedure. To begin, it is convenient to write the elements of the single particle density matrix in center of mass and relative coordinates:

$$\mathbf{R} = \frac{\mathbf{x} + \mathbf{x}'}{2} \quad \text{and} \quad \mathbf{r} = \mathbf{x} - \mathbf{x}'. \quad (3.14)$$

The normal density then takes on a familiar structure corresponding to the Wigner distribution [55]

$$\begin{aligned} G_N(\mathbf{R}, \mathbf{k}) &= \int d^3r \langle \chi_a^\dagger(\mathbf{R} - \mathbf{r}/2) \chi_a(\mathbf{R} + \mathbf{r}/2) \rangle e^{-i\mathbf{k}\cdot\mathbf{r}} \\ &= \int d^3r G_N(\mathbf{R}, \mathbf{r}) e^{-i\mathbf{k}\cdot\mathbf{r}}, \end{aligned} \quad (3.15)$$

which, in the high-temperature limit, will map to the particle distribution function $f(\mathbf{R}, \mathbf{k})$ for a classical gas. Correspondingly, the anomalous density can be written in Fourier space as

$$\begin{aligned} G_A(\mathbf{R}, \mathbf{k}) &= \int d^3r \langle \chi_a(\mathbf{R} - \mathbf{r}/2) \chi_a(\mathbf{R} + \mathbf{r}/2) \rangle e^{-i\mathbf{k}\cdot\mathbf{r}} \\ &= \int d^3r G_A(\mathbf{R}, \mathbf{r}) e^{-i\mathbf{k}\cdot\mathbf{r}}. \end{aligned} \quad (3.16)$$

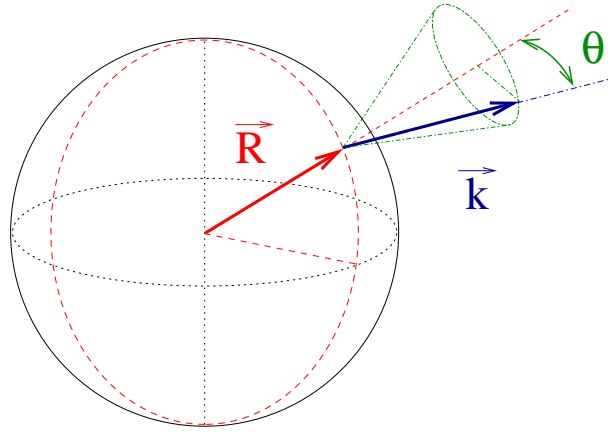


Figure 3.1: Illustration of the spherically symmetric geometry used as defined by the center of mass vector \vec{R} , relative momentum vector \vec{k} , and the angle θ between them.

In this geometry, the angular dependence of the center of mass vector \mathbf{R} is irrelevant, and the cylindrical symmetry about \mathbf{R} allows the wavevector \mathbf{k} to be represented by its length and the one remaining angle as illustrated in Figure 3.1.

This simplification allows us to represent the density distributions in three-dimensions as

$$G(\mathbf{R}, \mathbf{k}) = G(R, k, \theta), \quad (3.17)$$

where G corresponds to either the normal (G_N) or anomalous (G_A) density. It is now straightforward to rewrite Eqs. (3.9) and (3.10) in this coordinate system. It is worth pointing out the simple structure of the kinetic energy contributions to Eq. (3.10) which, for the G_N and G_A components, take the corresponding forms, respectively:

$$\left(\nabla_{\mathbf{x}}^2 - \nabla_{\mathbf{x}'}^2\right) G_N(\mathbf{x}, \mathbf{x}') = 2(\nabla_{\mathbf{R}} \cdot \nabla_{\mathbf{r}}) G_N(\mathbf{R}, \mathbf{r}) \quad (3.18)$$

$$\left(\nabla_{\mathbf{x}}^2 + \nabla_{\mathbf{x}'}^2\right) G_A(\mathbf{x}, \mathbf{x}') = \left(\frac{1}{2}\nabla_{\mathbf{R}}^2 + 2\nabla_{\mathbf{r}}^2\right) G_A(\mathbf{R}, \mathbf{r}). \quad (3.19)$$

One may now take the Fourier transform with respect to \mathbf{r} as indicated by Eqs. (3.15) and (3.16), replacing $\nabla_{\mathbf{r}} \rightarrow i\mathbf{k}$. The gradient operator $\nabla_{\mathbf{R}}$ can be expressed in any representation, but it is most convenient to use spherical polar coordinates aligned with

the \mathbf{k} direction vector

$$\nabla_{\mathbf{R}} = \hat{R} \frac{\partial}{\partial R} + \hat{\theta} \frac{1}{R} \frac{\partial}{\partial \theta} + \hat{\varphi} \frac{1}{\sin \theta} \frac{\partial}{\partial \varphi}, \quad (3.20)$$

where φ is the azimuthal angle about \mathbf{k} (which will eventually drop out in our chosen symmetry), and $(\hat{R}, \hat{\theta}, \hat{\varphi})$ are the spherical unit vectors in the R , θ , and φ directions. Noting that $\hat{R} \cdot \mathbf{k} = k \cos \theta$, $\hat{\theta} \cdot \mathbf{k} = -k \sin \theta$, and $\hat{\varphi} \cdot \mathbf{k} = 0$, we arrive at the following expression for the differential operator in Eq. (3.18):

$$\nabla_{\mathbf{R}} \cdot \mathbf{k} = k \left(\cos \theta \frac{\partial}{\partial R} - \frac{\sin \theta}{R} \frac{\partial}{\partial \theta} \right). \quad (3.21)$$

Furthermore, the spherical Laplacian for a system with no azimuthal dependence, as required in Eq. (3.19), is given by

$$\nabla_{\mathbf{R}}^2 = \frac{1}{R^2} \frac{\partial}{\partial R} \left(R^2 \frac{\partial}{\partial R} \right) + \frac{1}{R^2 \sin \theta} \frac{\partial}{\partial \theta} \left(\sin \theta \frac{\partial}{\partial \theta} \right). \quad (3.22)$$

In practice, we expand the θ dependence of G_N and G_A in terms of the orthogonal Legendre polynomials and the angular derivatives are then easily implemented via the usual recursion relations.

3.5 Numerical results and analysis

As an initial test, we expect the resonance theory to give a similar prediction to the Gross-Pitaevskii equation in the initial phase of the collapse, when the quantum depletion is small. Figure 3.2 shows a direct comparison between the Gross-Pitaevskii approach and the resonance theory. The same initial conditions were used for all our simulations: 1000 rubidium-85 atoms in the ground state of a 10 Hz harmonic trap. For all the images we present, the results of the three-dimensional calculation, in our spherical geometry, are illustrated as a two-dimensional slice through the trap center. In the Gross-Pitaevskii solution we used a scattering length of $-200 a_0$, where a_0 is the Bohr radius. For comparison, the Feshbach resonance theory uses a positive background

scattering length of $50 a_0$ and a resonance width and detuning, respectively, of 15 kHz and 2.8 kHz. These parameters give the same effective scattering length as the one used in the Gross-Pitaevskii evolution, but nowhere in the resonance theory does the effective scattering length appear explicitly. As is evident, there is no noticeable discrepancy between the two approaches over this short timescale. Eventually, we expect these theories to diverge significantly as the density increases and the coupling between the atomic and molecular degrees of freedom become stronger. However, at this stage, the agreement is a demonstration that our renormalized theory correctly allows us to tune the interactions in an inhomogeneous situation.

We now proceed to a more complex situation in which the timescales for the atom-molecule coupling and the collapse dynamics are more compatible. From a numerical point of view, it becomes convenient to increase the resonance width to 1.5 MHz and the detuning to 14 kHz so that the effect of the atom-molecule coupling will appear in the first stage of the collapse. This allows us to form a complete picture of the dynamics involving the atomic collapse and the simultaneous coupling to a coherent molecular field. The numerical calculation is shown in Fig. 3.3 for both the condensed and non-condensed components. We see the formation of a significant fraction of non-condensed atoms—a feature not described within the Gross-Pitaevskii framework. During a time evolution of 0.8 ms the condensate fraction falls to approximately 80% of its initial value while the non-condensate fraction reaches a peak at around 20%. The amplitude of the scalar field ϕ_m remains below the 2% level at all times.

To better illustrate the behavior of the atoms during the collapse, we present the flow of the different distributions involved. The condensate velocity field is shown in Fig. 3.4. It exhibits similar characteristics to those predicted by the Gross-Pitaevskii theory, which, without loss, predicts that the condensed atoms will always accelerate toward the trap center. In contrast, the velocity field of the atoms outside of the condensate is radially outward.

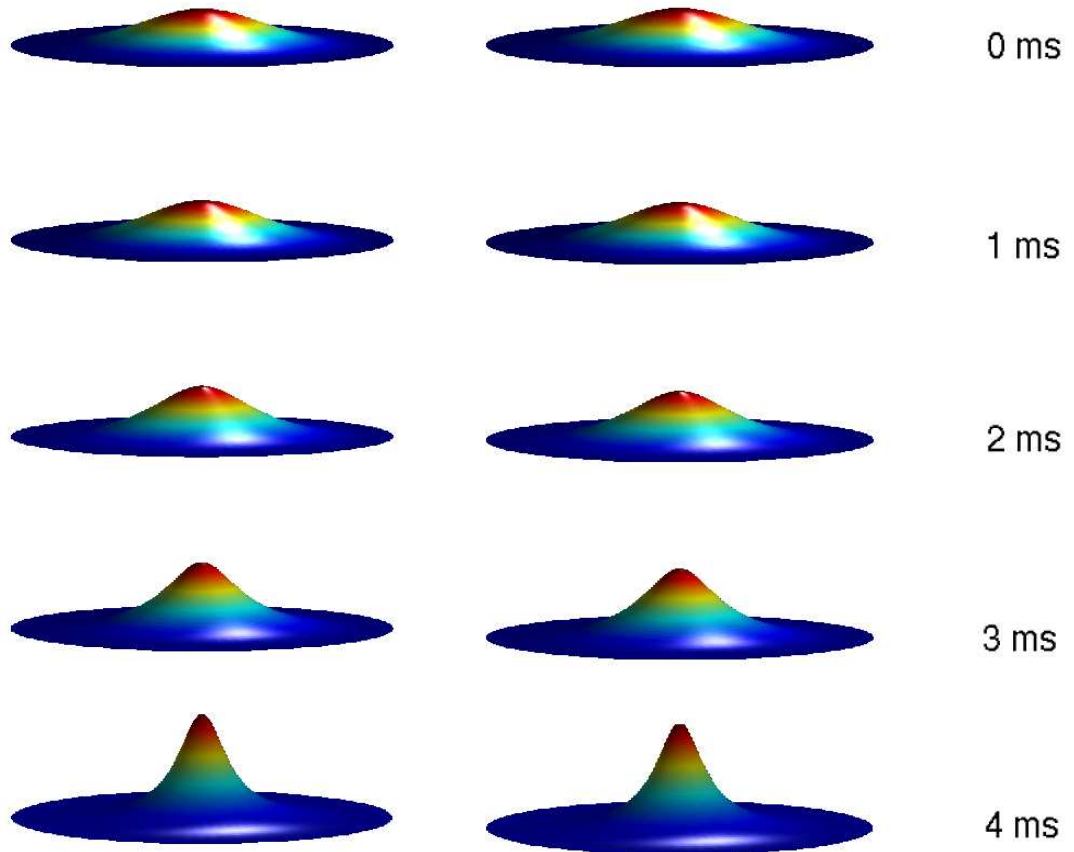


Figure 3.2: A direct comparison of the collapse between the Gross-Pitaevskii (left) and the resonance approach (right) within the regime of applicability of the Gross-Pitaevskii equation. Each horizontal pair is at the same time step with time increasing from top to bottom. As expected, we observe no appreciable difference between the two methods.

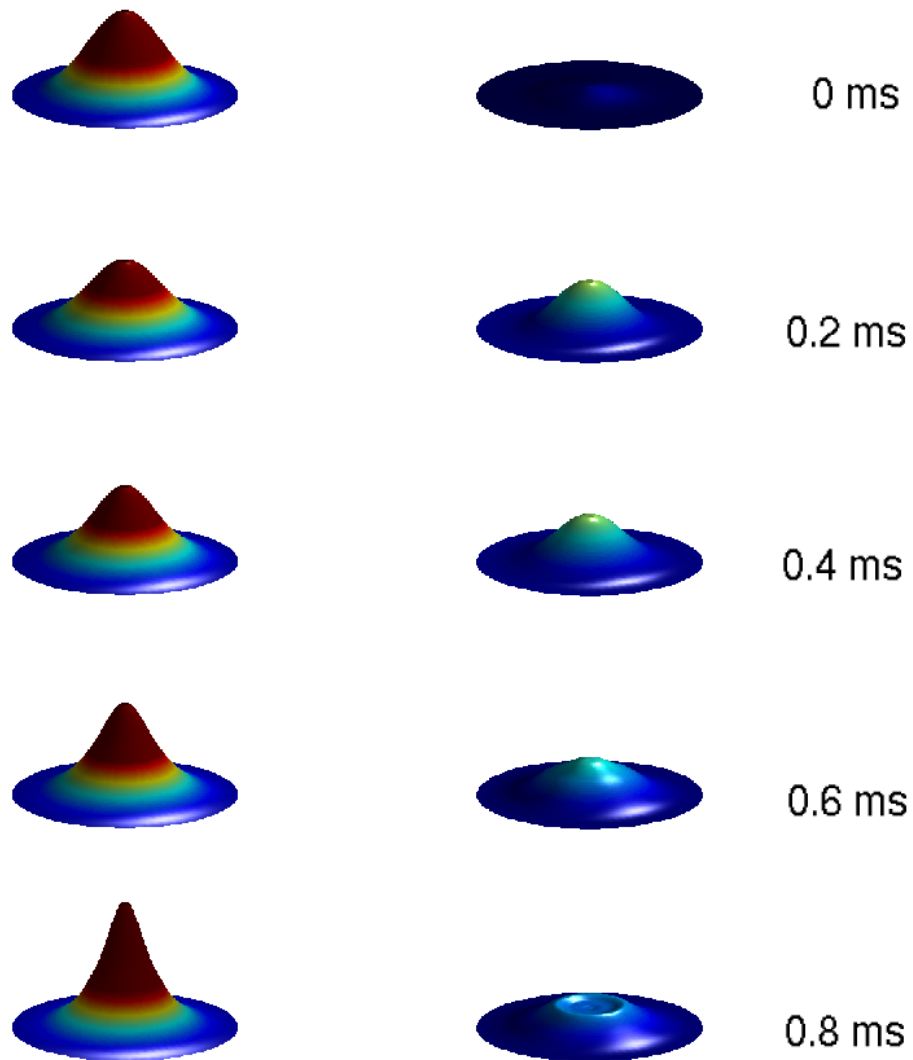


Figure 3.3: The simulation of the collapse in the resonance theory showing the time evolution of the condensed fraction $\phi_a(\mathbf{x})$ (left) and noncondensed fraction $G_N(\mathbf{x}, \mathbf{x})$ (right). Each horizontal pair is taken at the same instant of time with time increasing from top to bottom. It is evident that noncondensate atoms are produced during the collapse forming rings which propagate from the center of the cloud outward.

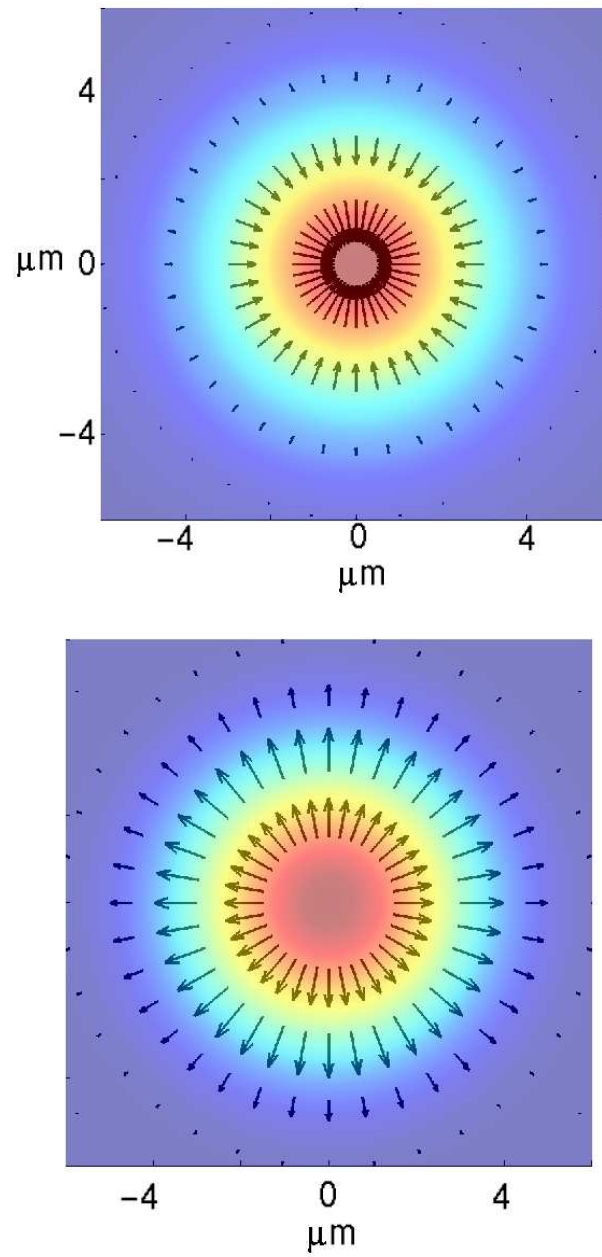


Figure 3.4: The velocity fields for the condensate component $\phi_a(\mathbf{x})$ (top) and the non-condensed component $G_N(\mathbf{x}, \mathbf{x})$ (bottom) midway through the simulation (0.4 ms). The color contours indicate the densities and the velocity fields are represented in direction and strength by the arrows. This clearly shows that in the resonance theory, as the condensate collapses inward, the non-condensate atoms that are generated flow outward.

An important quantity to calculate for these expanding non-condensed atoms is the effective temperature, or energy per particle, since this quantity is observed experimentally. This is illustrated in Fig. 3.5 where we show, superimposed on an illustration of the density, a colormap of the temperature. The hottest atoms generated in the center of the cloud are of comparable energy scale to those seen in the experiment, being on the order of 100 nK.

3.6 Conclusion

These numerical simulations illustrate the feasibility of generating atomic bursts purely through a coupling between an atomic and molecular component. However, there are a number of important distinctions with the experimental situation which would have to be accounted for before making a direct comparison. These simulations contain no inelastic three-body loss and particle number is absolutely conserved. In reality, three-body loss may be important to the experiment, but we suggest with this work that three-body loss is not the only mechanism for producing a non-condensed burst during the collapse.

It should be emphasized that, if our hypothesis for the burst generation is correct, the non-condensate atoms that are produced by this mechanism are not simply generated in a thermal component, but are instead generated in a fundamentally intriguing quantum state. The process of dissociation of molecules into atom pairs produces macroscopic correlations reminiscent of a squeezed vacuum state in quantum optics. This means that every atom in the burst with momentum \mathbf{k} would have an associated partner with momentum $-\mathbf{k}$. In principle, the correlations could be directly observed in experiments through coincidence measurements providing clear evidence as to whether this is the dominant mechanism for the burst generation in the Bose-nova.

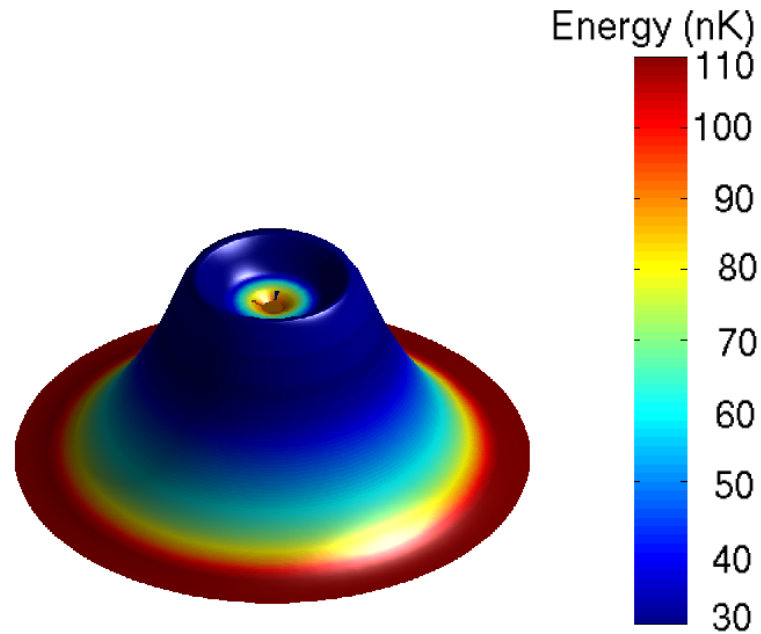


Figure 3.5: Density distribution of the non-condensate atoms near the end of the simulation (0.8 ms) on which we have superimposed the energy per particle as a colormap. The range of energies, of order 100 nK, is consistent with the characteristic scale of the burst particle energies in the Bose-Einstein experiment. Note that hot atoms are generated in the center of the cloud during the atom-molecule oscillations since this is where the atom-molecule coupling is strongest (the coupling strength varies as the square root of the density). As the hot particles radiate outward a ring can be observed.